Chapter 1

Reweighting Dynamics by Collective Variables

Complex systems consist of many particles giving rise to multiple pair and higher order interactions. The large number of interactions is burdensome to analyse and display for interpretation. One typically reduces the high-dimensional space to a few low-dimensional variables describing the slowest dynamical processes of the system. Examples are the description of a magnet by its magnetisation and ignoring the influence of local dipole fluctuations [16] or the crystallisation of particles described by the closest radial environment of each crystallising particle [12]. Fast and local processes are integrated out when deciding for a set of collective variables. This is compatible with MSM construction because fast processes are neglected too. However the mesoscopic descriptors or *collective variables*(CV) are chosen system-specific and the choice limits the view on the system: The crystallisation described by the local environment of the particles holds detailed view on the crystalline phase but limited information on the liquid phase. Furthermore, a poor choice can hide important processes or cause an inaccurate estimation of implied timescales [2, 9, 17]. Dimensionality reduction and choosing an advantageous set of collective variables is a widely discussed research field of its own and is applied to describe complex systems in chemistry, biology, physics and more [13].

MSM require the use of CV tp be computationally accessible. Up-to-date MSMs use $10^2 - 10^3$ microstates [10], resulting in $10^4 - 10^6$ possible transitions that have to be sampled. A construction on the full conformational space requires a larger

number of transitions that would exceed computational boundaries. The description by collective variables allows us to bypass these limitation. This chapter tests the reweighting procedure on systems described by collective variables to extend its scope to a larger group of systems. The reweighting method is first applied to a particle in a 2D-potential described by 1 dimensional collective variable. The second test system is a course-grained tetraalanine model being described by CV and showing many-body interactions.

1.1 Single Particle in Collective Variable Space

As a first testing ground we choose the 2D system from section **??** and integrate out the $y-$dimension orthogonal to the driving force, shown in figure 1.1a,b. This will imitate the reduction to a collective variable on the testing ground of the well-understood minimal system. A MSM is constructed on the reduced space and the reweighting procedure is tested without adjustments.

The 2-dimensional system in section is reduced by integrating along the $y-$axis of the system. A mean force and mean potential is calculated by

$$\begin{aligned} \langle \mathbf{F}(x) \rangle &= \int \mathrm{d}y \, \mathbf{F}_{\mathrm{2D}}(x,y)\pi(x,y) \\ \langle U(x) \rangle &= \int \mathrm{d}y \, U_{\mathrm{2D}}(x,y)\pi(x,y). \end{aligned} \tag{1.1}$$

Note that the definition of the mean potential is only valid for the equilibrium system and has undetermined physical meaning for NESS. The position of the metastable states are determined from the x-coordinate of the 2D system to compare the dynamics of full and reduced system. The dimensional reduced data are collected during runtime of the full systems simulation. An MSM is constructed with the same lagtime $\tau = 0.02 \; \mathcal{T}$ and the same 30 equi-sized microstates in x-direction.

Figure 1.1c,d compares the FPTD and the stationary distribution of the reduced system in equilibrium and under driving of $9\frac{\epsilon}{\mathcal{L}}$ when reweighting the systems into each other. The FPTD of the 2D system is shown for comparison. Small deviations are seen in the FPTD, but are of the same order and type as the reference 2D system. The reweighting for short processes of $1-5 \; \tau$ are overestimated, the peak underestimated in both cases. The tail for longer processes is reweighted correctly.

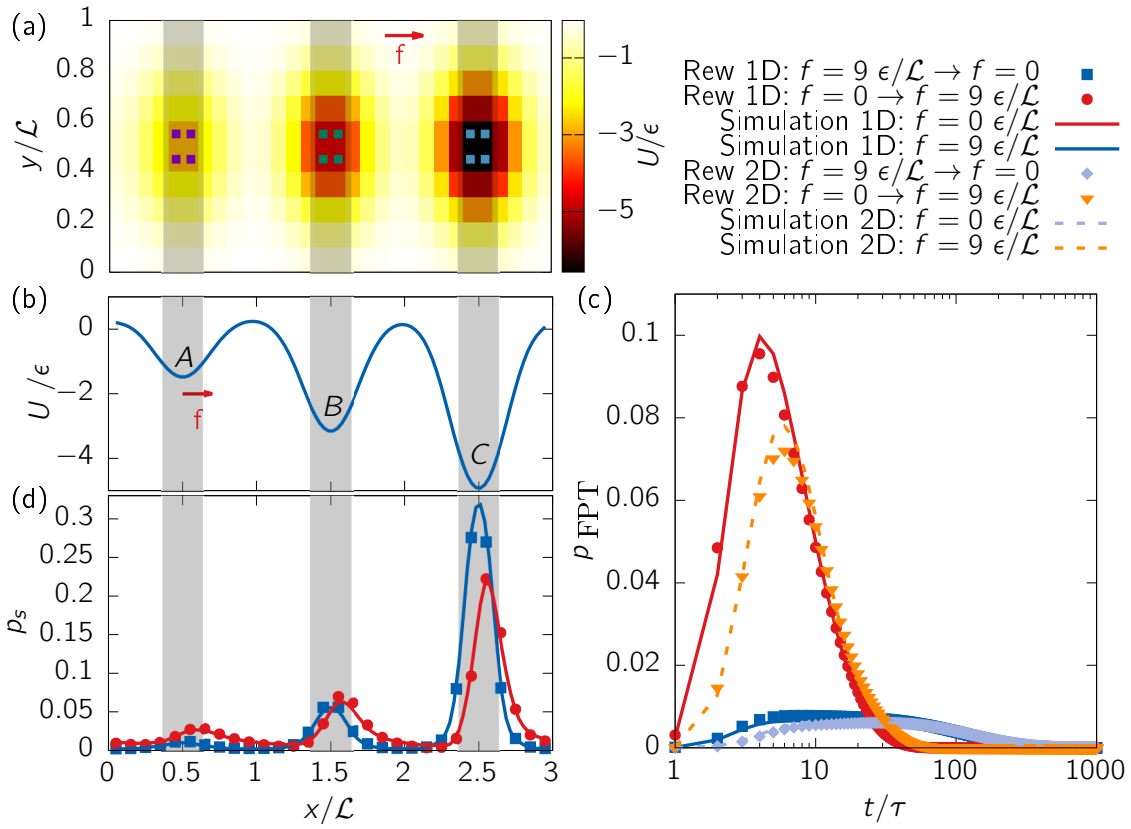

Figure 1.1: (a) The 2D potential with the three metastable states indicated by squares. Integrating out the $y-$dimension gives the (b) the mean potential of the equilibrium system. The grey area represents the new metastable states A,B,C. The area of the metastable state is effectively increased. (d) The stationary distribution of the reduced system and (c) FPTD of the process $C \to B$. The lines in (c,d) represent the results from simulating a single particle without (blue) and with (red) external force. The dots are the results from reweighting the systems into each other. The orange and silver-blue dashed lines show the same process for the underlying 2D process with dots representing the reweighted FPTD.

The reweighting works well on the stationary distribution of the 1D system. We deduce that the reweighting works well, even though systems details or lost by the used collective variables. An impairing effect on the reweighting cannot be seen for this system. The mentioned deviations are based on deviations on the underlying 2D-system.

Figure 1.3 shows continuous reweighting from the equilibrium system for the first three moments of the FPTD between metastable states and the occupation probability of each metastable state. Additionally the reweighting from the underlying 2D system is shown by dashed lines. We focus on comparison of results of 2D and its reduced system first. The MFPT is responding to external driving the same in both systems. The processes along the driving speed up immediately, the processes opposing the driving slow down at first, before the spatially longer path along the external force becomes more probable and the process speeds up too. For all processes the 2D process is slower than the dimensional reduced process. This effect of accelerated dynamics is universally known from coarse-graining different materials [3,5,8,14]. It originates in the disappearance of roughness in the free energy surfaces, resulting in a decrease of effective friction and increase of effective mobility. For our simplified model, this effect reduces the potential barrier between the barriers, leading to the acceleration of the coarse-grained process. The response of full and reduced processes under driving remains the same although mobility was not preserved.

The variance of the FPTD of the reduced system is lower compared to the 2D system. This agrees with the observation that MFPT and variance behave similarly. The skewness of both systems agrees in both systems. A deviation of the full and reduced system is seen in the inset of the skewness for process $A \to B$. The initial increase in skewness was seen for different systems in section **??** based on low discretisation of the FPTD for fast processes. The following drop of skewness was unique for the 2D system and is explained by emergence of another peak of slow processes in the FPTD. This class of processes was identified with trajectories bypassing the metastable state due to heavy driving. This effect of bypassing a metastable state cannot occur in the 1-dimensional description. Figure 1.2 shows the FPTD of the reduced system under driving does not show a second peak. The decrease around $6\frac{\epsilon}{\mathcal{L}}$ of the skewness is based on a summarising effect on the FPTD of stronger driving. The deviation in skewness of the 2D and is reduced system is thus based on loosing information on the dynamics.

The occupation probability of the metastable states is considerably larger for the reduced system. The metastable states in the 2D system are smaller because they do

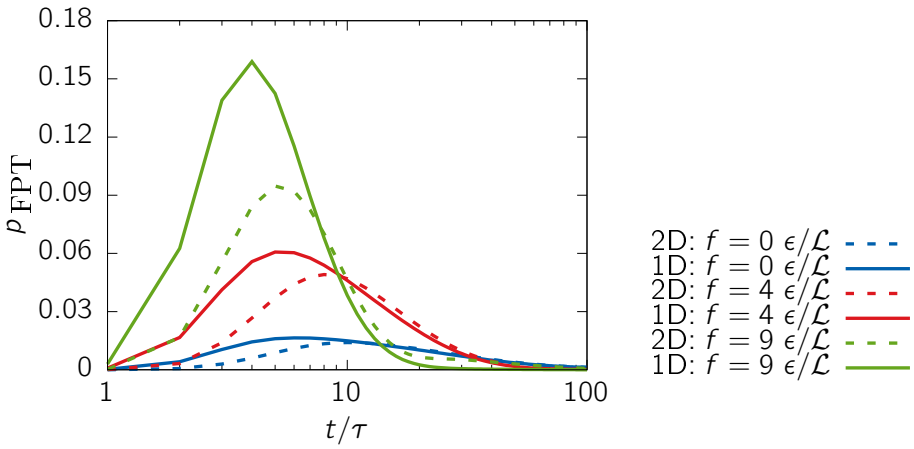

Figure 1.2: FPTD of transition $A \rightarrow B$ simulated at 3 different driving forces. Increased driving promotes short-time processes and suppresses slow processes. The continuous lines show the FPTD for the reduced system, the dashed lines for the underlying 2D system.

not span the whole y-direction. The reduction to the x-axis enlarges the metastable states effectively and the occupation probability increases. The trend of decreasing occupation in C and increase in A and B is the same for both systems.

We will now turn to the deviation between simulation of the reduced system and its reweighted properties. The largest deviation can be seen for the process $A \rightarrow B$, but it is comparable to the deviation of the 2D system for this process, shown in figure **??**. The same observation is made for the deviation in occupation probability of state C. The error of the reweighting are much smaller for the other processes. In general the deviations are all of the same shape and relative quantity as for the underlying 2D process. We conclude that the use of collective variables of the system did not affect the reweighting process and it can be applied to the same extend as the reweighting on configurational space. Deviations of the reweighting are adopted from the underlying errors in configurational reweighting and were discussed in section **??**.

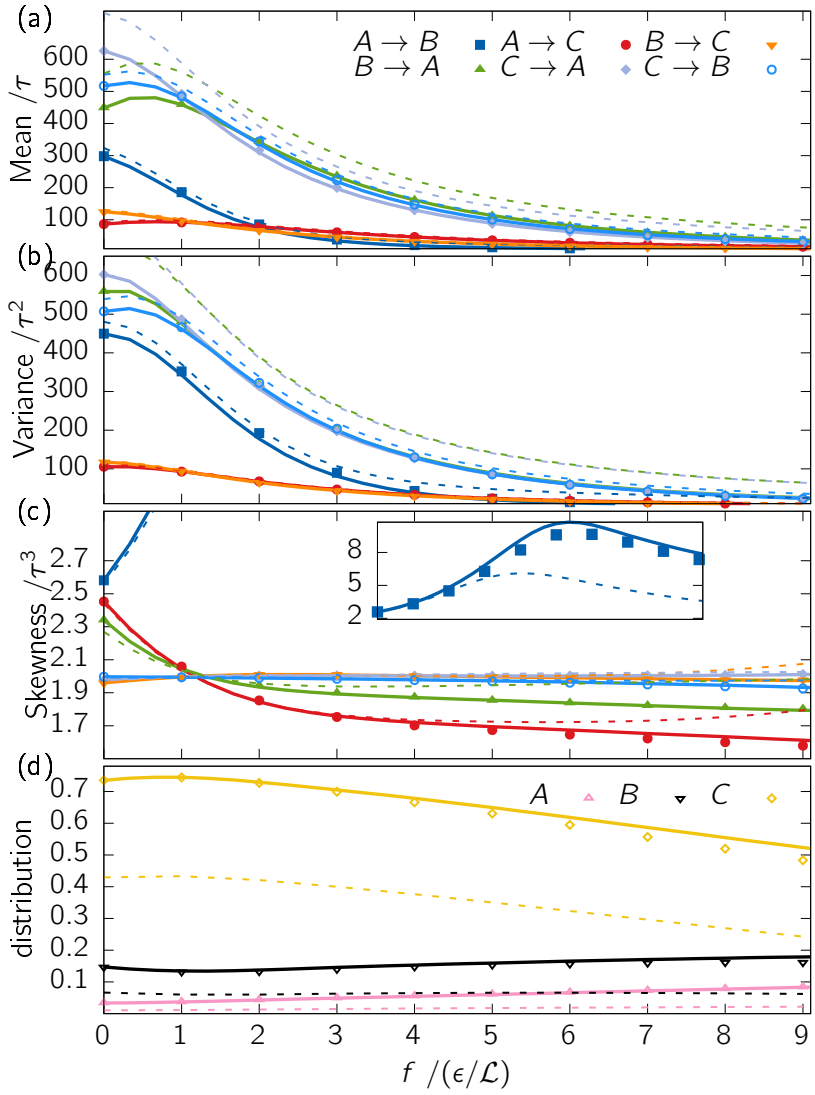

Figure 1.3: (a-c) The first three moments of the FPTD for all six processes between metastable states defined in figure 1.1 under varying external force f. (d) The occupation probability of each metastable state. The dots represent the value measured from simulation. The line is the equilibrium system continuously reweighted. The dashed lines are the processes of the underlying processes in 2D space.

1.2 Tetraalanine

This system is a coarse-grained tetraalanine peptide consisting of four beads. This model is the first non-artificial material and challenges the reweighting procedure by many-body interactions. External global forces are applied along the CVs to alter the dynamics. These forces may represent an optical tweezer controlling end-to-end distance. The choice of the CVs and the forces applied to the system are chosen by the user. The current forces are chosen to test the effectiveness of the reweighting procedure for conservative and non-conservative forces.

Tetraalanine is a peptide consisting of 44 amino acids and 52 atoms. Each amino acid is coarse-grained to one bead centered at the backbone of the peptide. The coarse-grained force field constructed by Rudzinski and Noid [15] for the molecule solvated in water consists of 3 pair potentials along the backbone, 2 bending interactions between 3 subsequent beards, a dihedral angle φ between all 4 beads and interaction between the first and the last bead R_{14}. The bending interactions are defined by the angle formed between the lines of the first two and last two beads. The dihedral angle is defined by the angle between the planes formed by the first three and last three beads. The Markov State Model is constructed using the end-to-end distance R_{14} and the dihedral angle φ as CVs, following the example of Bereau and Rudzinski [1]. The system will be driven with constant force along both CVs in both directions. The unperturbed system is called the reference system.

The free energy surface of the reference system is shown in figure 1.5a. Three basins were identified using PCCA+ as introduced in section **??**, representing helical states H, extended state E and one intermediate state I. Note that the direction of driving makes a difference, because the free energy surface lacks the symmetry of the previous systems. The driving along R_{14} can be translated to an additional interaction potential. Systems driven by a force along it are still in equilibrium and can be analysed via the Eigenvalue decomposition of the transition matrix. Driving along the periodic dihedral angle φ will push the system in a NESS that can be analysed using FPTD.

The lagtime analysis is performed in figure 1.5b for the reference system and one system driven along R_{14}. We choose a lagtime of 200 fs to capture the two slowest processes of both systems. The second process is unaffected by the additional forces so it will not be hidden in timescales lower than the lagtime by moving to higher driving forces. The MSM was constructed with 15 microstates over the range $[-\pi, +\pi]$ in

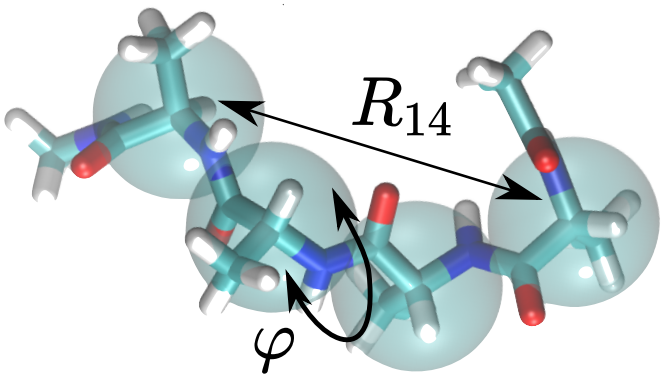

Figure 1.4: Atomistic and coarse-grained representation of Ala4. The rods show the atoms, where turquoise is C, white is H, blue is N and red is O. The transparent beads show the coarse-grained representation of the system. The end-to-end distance R_{14} and the dihedral angle φ are defined for the coarse-grained system.

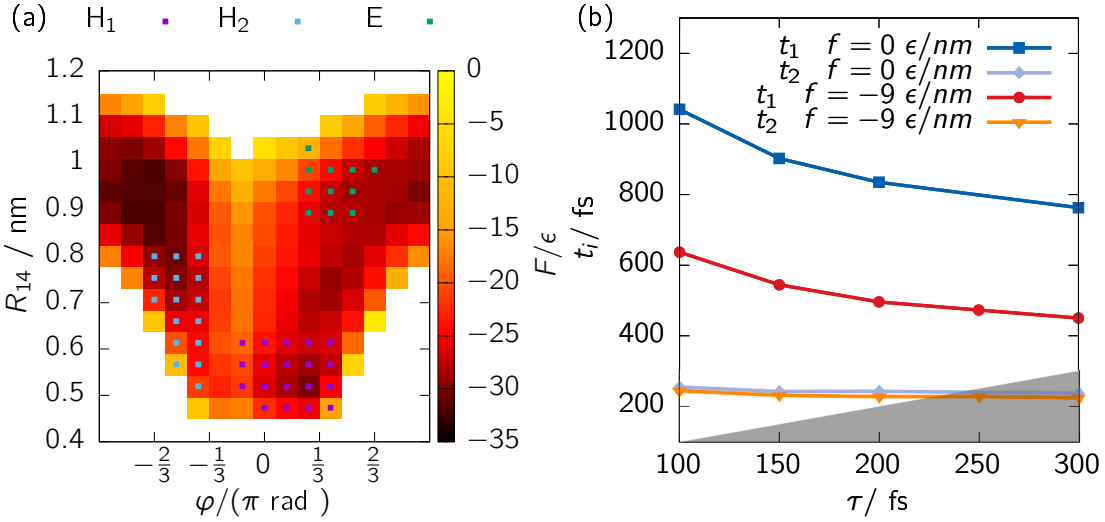

Figure 1.5: a) Free energy surface of Tetraalanine of the reference system. The metastable states are indicated by H,E,I. (b) Lagtime analysis of the system defined by the reference force field ($f_R = 0$) and driven along the end-to-end distance with $f_R = 9\frac{\epsilon}{nm}$. The shaded area marks the non-physical area where $t_i < \tau$.

φ-direction and 15 microstates in the range $[0.45\ nm, 1.15\ nm]$ in R_{14}-direction. Two additional sets of microstates were added to collect end-to-end distances outside this range. Energies are given in $\epsilon = \frac{kJ}{mol}$ and the system was simulated at temperature $T = 2.479\ \frac{\epsilon}{k_B}$.

1.2.1 Modifying End-to-end Potential

An optical tweezer use optical traps to confine beads of a single molecular in harmonic potentials [6]. We may predict the outcome of such an experiment by applying harmonic potential of varying strength between the first and the last bead and calculate the effects on statics and dynamics on Ala4 by reweighting from the undisturbed system. The forces applied are conservative, so this is an example of reweighting along CVs between equilibrium systems.

At first we have a detailed look at the Eigenvectors in figure 1.6 for the system at reference and for driving along R_{14} in negative direction with $f = -9\ \frac{\epsilon}{nm}$. The unperturbed systems stationary distribution shows highest probability at a state with ≈ 0.9 nm end-to-end distance and dihedral angle $\varphi \approx -0.8\ \pi$, this is associated with an extended state. The second minimum can be seen for $\varphi \approx\ 0.3\pi$ and $R_{14} \approx 0.5\ nm$, being associated with a helical state. A third smaller basin is found at an extended state ≈ 0.9 nm and an dihedral angle of $0.6\ \pi$. The slowest process describes the transition between the highly populated extended state and the helical and less populated extended state. It describes the transition over the large barriers around 0π or 1π. This second slowest process describes a transition for $\pi > 0$ on the right-hand side of the large barrier in the middle, between the helical state and the less populated extended state.

Focusing on the effect of the driving, the stationary distribution is pushed to the folded state because the ends are forced together. The basin of the helical states is higher populated. The slowest process changes, the polymer folds directly in the helical state at low R_{14}, as shown by the first Eigenvector. The second extended state at $0.6\ \pi$ is less important for this process when the additional force is applied. The timescale indicates that the folding occurs faster. The second slowest process is not affected by the driving and still described the transition on the right-hand side of the centered barrier. We note that reweighting to the driven system from the reference system recovers this detailed view on the slowest process correctly.

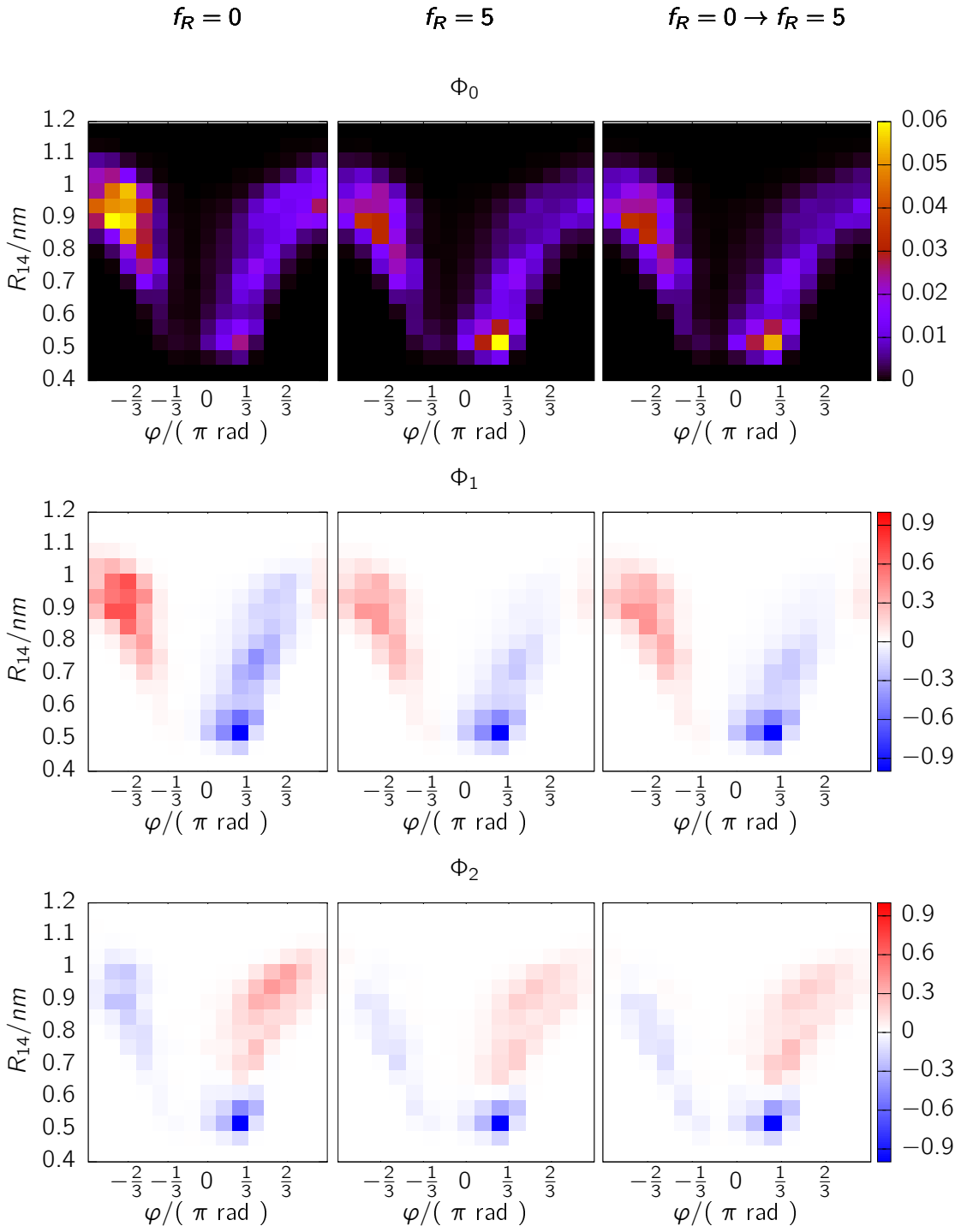

Figure 1.6: The first row shows the stationary distribution, the second row the first Eigenvector and the third row the second eigenvector of three systems. The system in the first column is the non-perturbed reference system, in the second column the perturbed system at $f = -9\ \frac{\epsilon}{nm}$ and in the third row the reweighted system from reference.

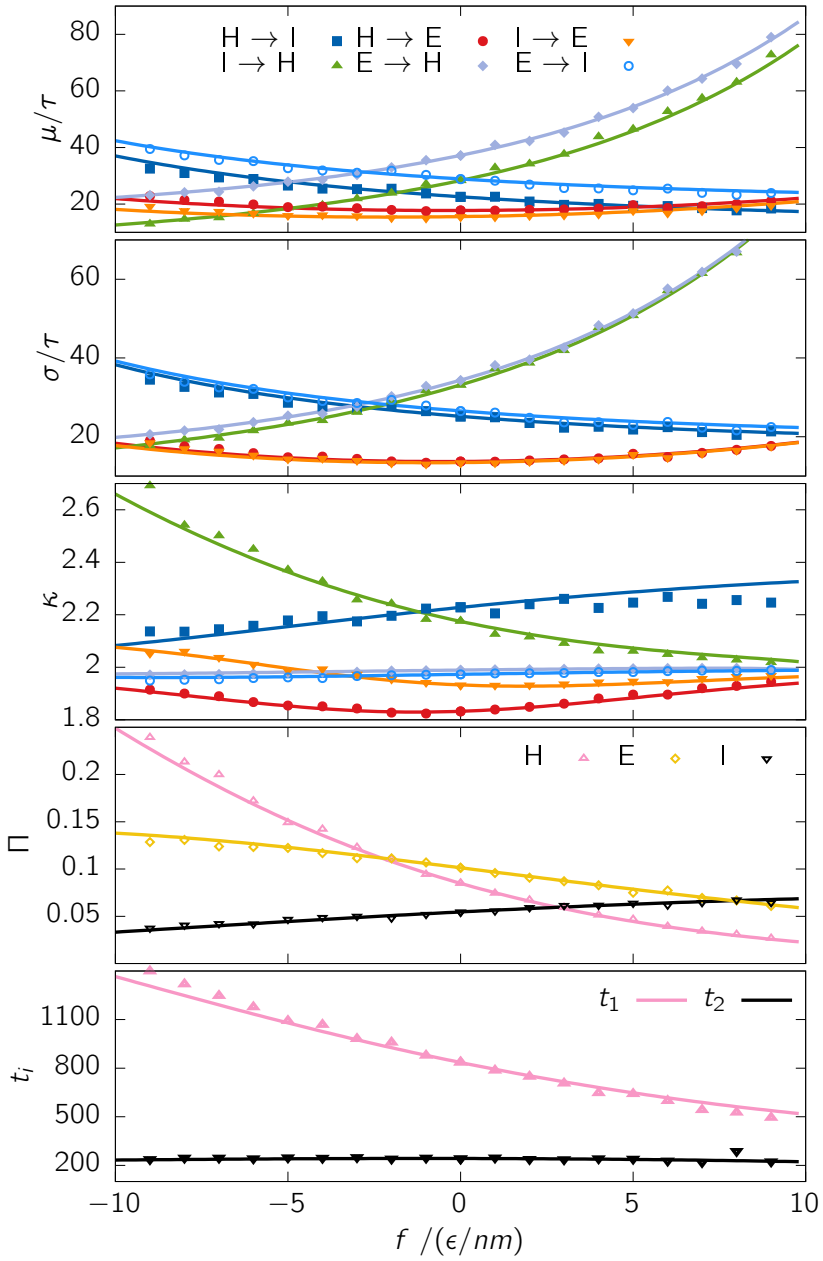

Figure 1.7: (a-c) The first three moments of the FPTD for all six processes between metastable states defined in figure 1.5 under varying external force f. (d) The occupation probability of each metastable state. (e) The timescale of the two slowest processes covered by the MSM. The dots represent the value measured from simulation. The line is the reference system continuously reweighted.

Figure 1.7 shows the first three moments of the FPTD between the metastable states as defined in figure 1.5a. The metastable states as defined by PCCA+ do not coincide with the states highlighted for the Eigenvectors. State H can be associated with helical states, located right of the free-energy barrier at $\varphi \approx 0.15\ \pi$. State I is an intermediate state at $\varphi \approx 0.3\ \pi$. The global basin at extended state is not covered by the choice of PCCA+ because it is dynamically unstable. Nevertheless, we call the state identified below extended state E. Transition from H or E to the intermediate state I slow down for attracting end-beads (negative forces) and speed up for repulsive end-beads (positive forces). The inverse happens for the processes from E or I to folded state H. Attractive end-beads increases the speed of these processes, driving to elongated states reduces it. H is the more stable configuration because the end-beads can be close together. Transitions to extended state E are comparable unaffected by the driving. Looking at the stationary distribution in figure 1.7d shows an increase in population of intermediates state I under repulsive end-beads. It allows the end-beads to be far apart, so it becomes higher populated than H. The intermediate state I and extended state E change linearly in probability with changing end-to-end attraction, the state H exponentially. The variance behaves proportional to the MFPT. The variance shows minor changes under driving but does not show peculiar effects as seen for previous systems. The comparison is extended by the first two timescales of the system. The fast timescale depends strongly on the driving, the second timescale is unaffected as we have observed in the lagtime analysis. Since all systems under observation are in equilibrium we do not expect special dynamical effects because the dynamics are governed by accustomed detailed balance.

The reweighting method works well for the Tetraalanine system driven by a constant conservative force. It is concluded that dynamics can be reweighted along the CV even if complex interactions of many bodies are involved.

1.2.2 Driving along Dihedral Angle

We will now turn to a driving along the dihedral angle. This is a circular motion with periodic boundary conditions giving rise to a NESS. While this motion is artificial for the Ala4, such circular motions are essential for molecular rotary motors, where the rotation is driven by ATP-synthesis giving rise to a unidirectional motion of the molecule [4].

The system is driven along the dihedral angle in both direction. Figure 1.8 gives

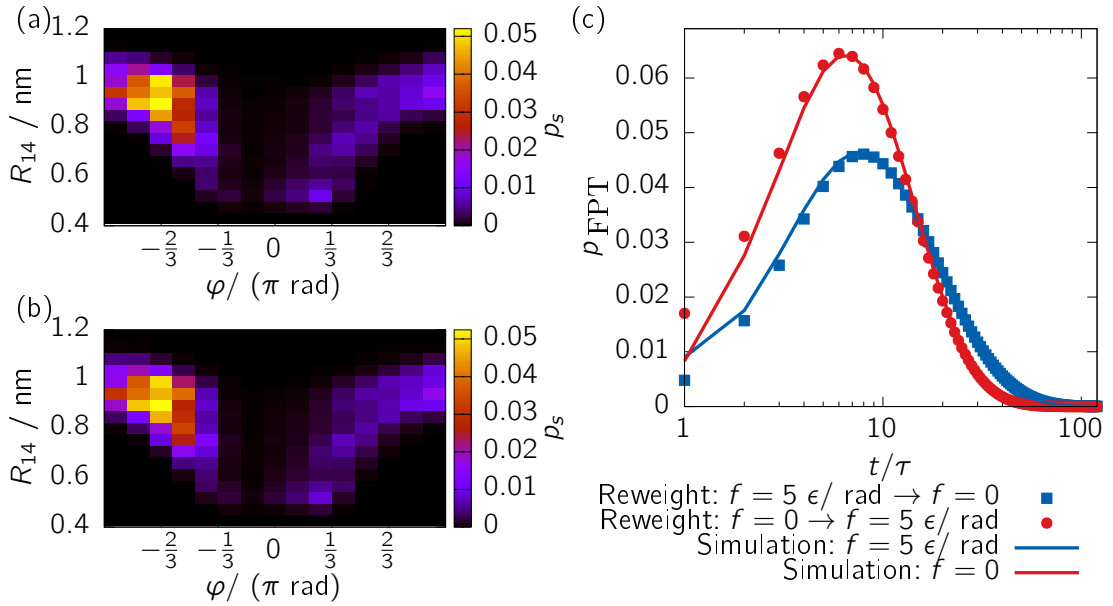

Figure 1.8: (a) Simulated stationary distribution at $f = 0.8\frac{\epsilon}{\mathrm{rad}}$. (b) Reweighted stationary distribution from reference to $f = 0.8\frac{\epsilon}{\mathrm{rad}}$. (c) FPTD of driven and reference system for transition $H_1 \rightarrow H_2$. The lines show data from simulation, the dots are from reweighting the systems into each other.

a detailed look at the system driven with $f = 0.8\frac{\epsilon}{\mathrm{rad}}$. We note that the unfolded states are more populated than before and states to the right of the barrier are less populated. The FPTD distribution from helical states H to the helical state E is shown and captured by the reweighting procedure. Deviations can be seen for short processes of length 1τ.

Turning to figure 1.10 shows the driving along φ in both directions. The dynamics of the system is largely dominated by the its large centered free-energy barrier. Driving in positive direction, the processes H $\rightarrow$ E and I$\rightarrow$E become faster as they are connected along the periodic boundary. The process I$\rightarrow$H slows down as it opposing the force. H $\rightarrow$I on the other hand becomes slower despite it is connected along the external force. The trajectories bypass the state I under driving more frequently. The transitions I $\rightarrow$H and E $\rightarrow$H are not correctly recovered for larger driving by the reweighting. The dynamics slow down for simulation and reweighting for low forces as expected. The simulation show that the slowing down reaches a peak after a while because the large barrier is crossed more frequently. The reweighting

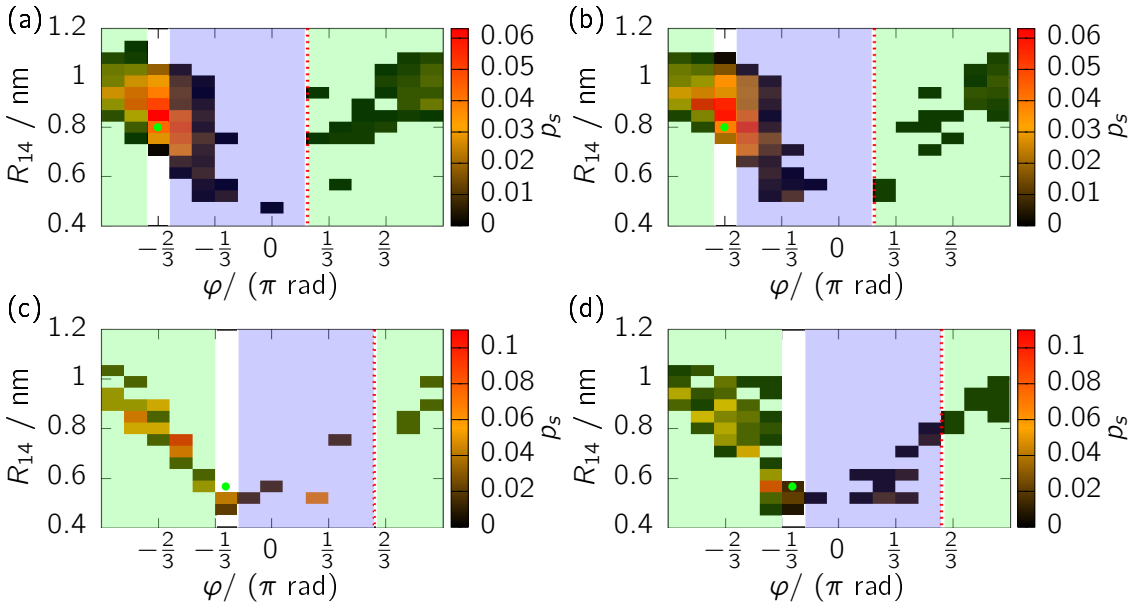

Figure 1.9: Transition matrices, starting at the state marked by the green dot. The transition matrices left (a,c) show the reference systems, the right (b,d) show a system driven by $1.4\frac{\epsilon}{\text{rad}}$. The red line represents the discontinuity in local entropy productions, starting from the green-marked state. All states shaded green are connected to the starting state by trajectory going left, all states shaded green are connected by a trajectory going right.

procedure has problems capturing this effect correctly although it worked well for the single particle models. The variance follows the behaviour of the mean again and the skewness indicates that the reweighting works well for $|f| < 1\frac{\epsilon}{\text{rad}}$. Driving in negative direction the effect on dynamics is inverted, the processes aligned with the force speed up, the processes opposing are slowing down. The process H→I is a special case again, because its getting faster too. The trajectories normally bypassing the state are now pushed into visiting the state. This is indicated by the increasing population of intermediate state I under negative driving and depopulation under driving positive driving. The helical state population shows the same behaviour, the extended state shows inverse population. The populations are recovered well by the reweighting, despite the deviations in the dynamics.

The reason for the described error lies in the local entropy productions. The correct choice is determined by the external force and the set of path connecting every pair

of microstates with each other. This connection of two microstates was easy to find for the previous system because they were separated by three or more barriers, as discussed in section **??**. It was easy to determine if the collection of path were directed with or against external forces. For equilibrium systems the path dependence is dropped, so the problem did not occur for driving in R_{14}-direction. This model on the other hand is driven to a NESS and shows only one major barrier along the dihedral angle. Choosing the correct local entropy production is more challenging here. For every jump in the Markov Model we have to decide if the underlying trajectory is aligned or directed against the external force. One way is to analyse the trajectories as will be shown in section **??**. Often one can deduce these information from the transition matrix, as demonstrated in figure 1.9a for the reference system starting at a state close to the global minimum. All states to the right of the starting point are expected to emerge from trajectories in positive φ-direction, all states to the left in negative φ-direction, taking periodic boundaries into account. In between these sets of trajectories is an area where no transition occurs. The lagtime of the MSM was chosen small such that these transitions do no take place. We are not able to tell if the transitions occurred via a path going to the left or the right. This empty space acts as a dividing line between the two sets of trajectories, marked by the red dashed line. The connection between the states in the transition matrix indicate, where to define the discontinuity in local entropy productions. Figure 1.9b shows the transition matrix with driving of $f = 1.4\frac{\epsilon}{\text{rad}}$ from the same starting point as before. The transition probabilities change by the driving but the spatially long transition are still forbidden. We are able to tell if the transition took a path in negative or in positive ϕ-direction. This is essential for the reweighting algorithm to work. To understand this, it helps to look at figure 1.9c,d for the same systems, but at a starting point left to the large central barrier in φ-direction. The space can be separated in transition in positive and negative ϕ-direction for the reference system as described before. For the driven system however, we cannot decide if the markovian jumps occur from hopping over the barrier or following a path around the periodic boundary. It might be that the microstates are connected by both sets of path. This makes it impossible to calculate the change in local entropy productions. Only if the set of paths are well-separated this is easily possible, as demonstrated for the first starting point. This is the source of the deviation seen in figure 1.10 for heavy driving.

We deduce that the reweighting along the dihedral angle will be limited for the present system. The set of path connecting two microstates should consist of similar trajectories for reference and target system. Unfortunately the current system with

a single large barrier makes this difficult. Furthermore, one cannot know in advance when this conditions is not met anymore. The small gaps between the groups of trajectories in Figure 1.9a,b are a warning signal. Models with three or more barriers, as constructed as a toy model, are less susceptible by this problem. A particle crossing a barrier is expected to take the short path over one barrier and is unlikely to hop over two barrier within one lagtime. We may suspect that this problem occurs more frequently by small models with only few particles and less complex free energy surfaces.

A possible way of solving this problem is by shortening the lagtime of the MSM. Shorter lagtimes result in shorter trajectories and shorter jumps. The reweighting procedure could be applied in a wider range. Unfortunately, figure 1.5 shows that smaller lagtimes show non-markovian dynamics. At the same time, increasing the number of microstates does not allow us to choose smaller lagtimes. Other choices made to construct the MSM are the CVs and the microstates. We may choose a different second CV when reweighting along the first. Such choices have great impact on the system and solve the problem of missing free-energy barriers. The microstates in the present model are chosen in equal size along the CVs. Advanced clustering techniques like k-means [7] or k-medoids [11] help to define more complex sets of microstates that would allow to reduce the lagtime. Both, the choice of CVs and the way of clustering the CV influence how dynamics are described by the MSM. We noted that the connection of two microstates should be described by a unique bundle of paths. This means that the CVs and its separation in microstates should be chosen to reflect underlying kinetic distances of the system. The same requirement for reweighting of dynamics in equilibrium was noted by Voelz et al. [18].

We conclude that the reweighting procedure works for complex many-body-systems described by CVs. We show how the reweighting can be applied for conservative or non-conservative forces along the chosen CVs similarly. These forces might emerge from optical tweezers, molecular motors, mechanical dragging or any other type of disturbance. The reweighting is based on the MSM being able to reflect the underlying dynamics of the system and by avoiding multiple sets of paths connecting two microstates.

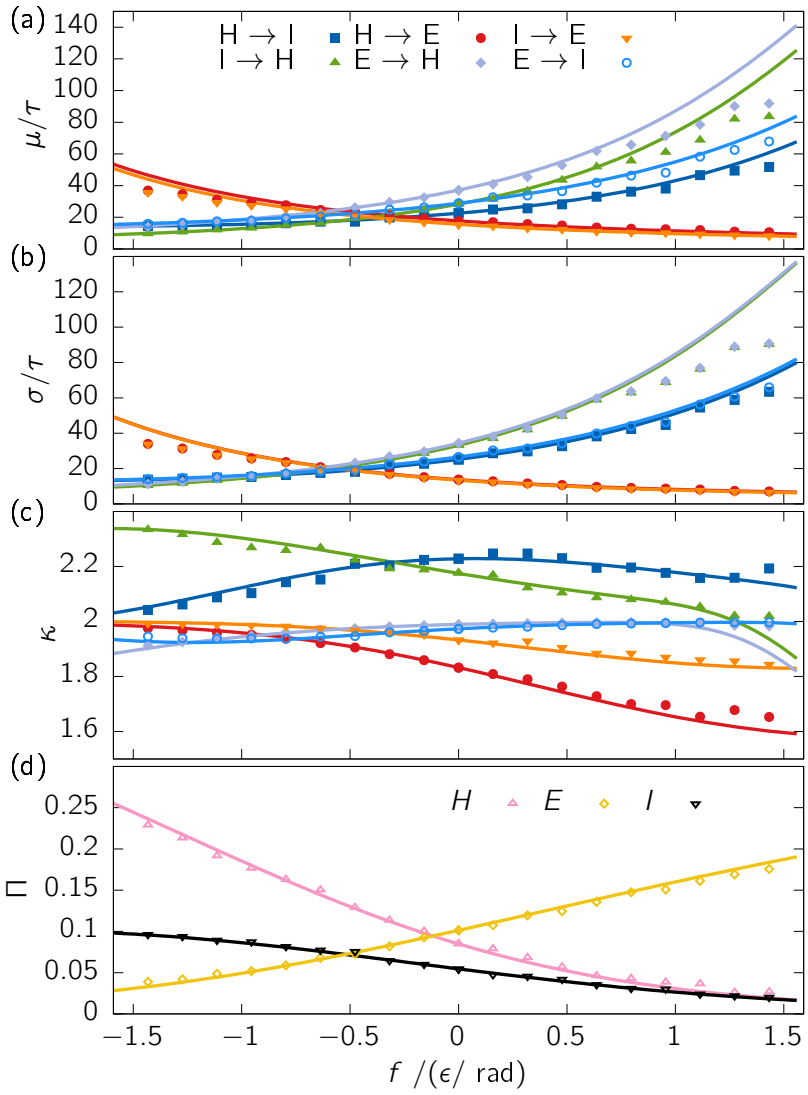

Figure 1.10: (a-c) The first three moments of the FPTD for all six processes between metastable states in figure 1.5 under varying external force f. (d) The occupation probability of each metastable state. The dots represent the value measured from simulation. The line is the reference system continuously reweighted.

Bibliography

[1] Tristan Bereau and Joseph F Rudzinski. Accurate structure-based coarse graining leads to consistent barrier-crossing dynamics. *Physical review letters*, 121(25):256002, 2018.

[2] Peter G Bolhuis, Christoph Dellago, and David Chandler. Reaction coordinates of biomolecular isomerization. *Proceedings of the National Academy of Sciences*, 97(11):5877–5882, 2000.

[3] Praveen K Depa and Janna K Maranas. Speed up of dynamic observables in coarse-grained molecular-dynamics simulations of unentangled polymers. *The Journal of chemical physics*, 123(9):094901, 2005.

[4] Robert H Fillingame. Molecular rotary motors. *Science*, 286(5445):1687–1688, 1999.

[5] M Guenza. Thermodynamic consistency and other challenges in coarse-graining models. *The European Physical Journal Special Topics*, 224(12):2177–2191, 2015.

[6] Junyi Jiao, Aleksander A Rebane, Lu Ma, and Yongli Zhang. Single-molecule protein folding experiments using high-precision optical tweezers. In *Optical Tweezers*, pages 357–390. Springer, 2017.

[7] Aristidis Likas, Nikos Vlassis, and Jakob J Verbeek. The global k-means clustering algorithm. *Pattern recognition*, 36(2):451–461, 2003.

[8] Melissa K Meinel and Florian Müller-Plathe. Loss of molecular roughness upon coarse-graining predicts the artificially accelerated mobility of coarse-grained molecular simulation models. *Journal of Chemical Theory and Computation*, 16(3):1411–1419, 2020.

[9] Frank Noé and Cecilia Clementi. Collective variables for the study of long-time kinetics from molecular trajectories: theory and methods. *Current Opinion in Structural Biology*, 43:141–147, 2017.

[10] Frank Noé and Edina Rosta. Markov models of molecular kinetics, 2019.

[11] Hae-Sang Park and Chi-Hyuck Jun. A simple and fast algorithm for k-medoids clustering. *Expert systems with applications*, 36(2):3336–3341, 2009.

[12] Ravi Radhakrishnan and Bernhardt L Trout. Nucleation of hexagonal ice (i h) in liquid water. *Journal of the American Chemical Society*, 125(25):7743–7747, 2003.

[13] Mary A Rohrdanz, Wenwei Zheng, and Cecilia Clementi. Discovering mountain passes via torchlight: Methods for the definition of reaction coordinates and pathways in complex macromolecular reactions. *Annual review of physical chemistry*, 64:295–316, 2013.

[14] Joseph F Rudzinski. Recent progress towards chemically-specific coarse-grained simulation models with consistent dynamical properties. *Computation*, 7(3):42, 2019.

[15] Joseph F Rudzinski and William G Noid. Bottom-up coarse-graining of peptide ensembles and helix–coil transitions. *Journal of chemical theory and computation*, 11(3):1278–1291, 2015.

[16] Jaroslav Tóbik, Roman Martoňák, and Vladimír Cambel. Free-energy landscapes in magnetic systems from metadynamics. *Physical Review B*, 96(14):140413, 2017.

[17] Omar Valsson, Pratyush Tiwary, and Michele Parrinello. Enhancing important fluctuations: Rare events and metadynamics from a conceptual viewpoint. *Annual review of physical chemistry*, 67:159–184, 2016.

[18] Hongbin Wan, Guangfeng Zhou, and Vincent A Voelz. A maximum-caliber approach to predicting perturbed folding kinetics due to mutations. *Journal of chemical theory and computation*, 12(12):5768–5776, 2016.